Enhanced oxidation resistance of Ti(C,N)-based cermets containing Ta

By E. Chicardi, F.J. Gotor and J.M. Córdoba*

Instituto de Ciencia de Materiales de Sevilla, Centro Mixto CSIC-US, Américo Vespucio 49, 41092 Sevilla, Spain.

Abstract

$(Ti_xTa_{1-x})(C_{0.73}N_{0.27})$–Co-based cermets with various Ta contents (x = 0, 0.01, 0.05, 0.1 and 0.2) were oxidized at 900 ºC for 48 hours in static air. The oxidation behavior was continuously monitored by measuring the weight change as a function of the oxidation time using a microbalance. A parabolic rate law, which is indicative of the formation of a protective oxide layer, was observed for all samples. The multi-layered oxide scale and the internal oxidation region that formed as the oxidation progressed toward the interior of the cermet specimens were characterized using XRD, SEM and EDS. The oxidation resistance of the studied materials was dramatically improved by increasing the Ta content. The enhanced oxidation resistance achieved in cermets with a Ta content of ~ 10 wt% may satisfy the optimal requirements for many applications in the field of cutting tools.

Keywords: solid-gas reaction, mechanical milling, oxidation, ceramic matrix composite

*Corresponding Author. E-mail: josem.cordoba@csic.es, Phone: +34 954 489217

1. Introduction

A key feature of cemented carbides and cermets, which are widely used in the cutting tools industry, is the potential to vary their compositions so that the resulting physical and chemical properties ensure high resistance to wear, deformation, fracture, corrosion and oxidation. Cermets are generally composed of hard ceramic grains based on Ti(C,N) embedded in a tough binder phase of Co or/and Ni. The hard ceramic particles generally have the characteristic core-rim microstructure, wherein the core corresponds to the original Ti(C,N) particles, and the rim is a carbonitride solid solution, $(Ti,Mt_1,Mt_2\ldots)(C,N)$, that is newly formed during the liquid-phase sintering. This solid solution contains Ti and other transition metals, which are added as binary carbides to the starting raw materials **[1-4]**.

Cermets possess good resistance to built-up edges, scaling and crater formation, and as a result, they are commonly used for high-speed milling, roughing and semi-finishing of carbon alloys and stainless steels. In cutting performance, Ti(C,N)-based cermets demonstrate improved surface finishing and tolerance control as well as prolonged tool life, even on superalloys and other difficult-to-machine materials **[5-7]**. During high-speed machining, work conditions are relatively extreme in terms of temperature and induced stresses, therefore requiring that the corresponding cutting tools exhibit excellent thermo-mechanical and tribological behaviors. The principal parameter to consider becomes the wear produced by the high temperatures in the cutting zone, which can reach values in the range of 800–1000 ºC **[8,9]**. Under these conditions, the high-temperature behavior is critical and more important than other mechanical properties, such as toughness and mechanical shock resistance, in determining the performance and lifetime of tools [**10**].

Ta and Nb are introduced into cermets as carbides (TaC, NbC) with the aim of improving the cermet properties at high temperatures, such as hot-hardness and high-temperature strength. It has also been observed that the resistance to crater wear and thermal cracking, which can occur during machining, is enhanced **[11]**. Although it is assumed that the good performance of Nb- and Ta-containing cermets at high temperature is attributable to an improvement in the oxidation resistance **[12]**, there is no available literature regarding the oxidation behavior of these types of cermets. Indeed, studies concerning the response to oxidation of Ti(C,N)-based cermets at high temperature in air is extremely scarce [**13-16**], despite the fact that it is a critical property for high-speed machining applications.

Based on the above considerations, in the present work, the oxidation resistance of a set of $(Ti_xTa_{1-x})C_{0.5}N_{0.5}$–Co-based cermets with varying Ta content was investigated at 900 ºC in static air. This work was possible because of the ability of the mechanochemical process known as mechanically induced self-sustaining reaction (MSR) to fabricate cermets that consist of complex carbonitride as the hard phase in a simple, direct and effective way [**17**]. The microstructure of the cermets before and after the oxidizing thermal treatment was analyzed with particular attention to the characteristics of the oxide scale and its evolution as a function of the Ta content. Comprehensive information concerning the kinetics and oxidation mechanism is also provided. This work demonstrates that the development of highly oxidation-resistant cermets is possible.

2. Materials and Methods

Cermets were fabricated using a pressureless sintering process from powders synthesized via MSR. Table I shows the nominal compositions of the cermets studied in this work. The experimental details of the MSR synthesis in a nitrogen atmosphere and the sintering process in an inert atmosphere have been described in a previous work **[18]**.

The isothermal oxidation was performed at 900 ºC (heating rate 20 ºC/min, free cooling) for 48 h in static air using a CI Robal electrobalance (C.I. Electronics Ltd.) attached to the support frame of a high-temperature vertical furnace (1500 ºC; Severn Furnaces Ltd.). Specimens with approximately similar dimensions (~ 3 mm×4 mm×5 mm) were placed on a platinum wire coil to maximize the contact of the surfaces with the surrounding atmosphere. For reliable comparisons, the specimens were cut from the central part of the sintered cermets.

X-ray diffraction diagrams were obtained using a PANalytical X'Pert PRO instrument equipped with a θ/θ goniometer using CuK_α radiation (40 kV, 40 mA), a secondary K_β filter and an X'Celerator detector. The diffraction patterns were scanned from 20° to 90° (2θ) in a step-scan mode at a step of 0.02° and a counting time of 275 s/step. The polished cross sections of the cermets before and after oxidation were examined via scanning electron microscopy performed on a Hitachi S-4800 SEM-FEG microscope. The metal content in the ceramic and binder phases and in the oxide scales was measured via energy dispersive X-ray spectrometry (EDS) with detectors (Bruker) coupled to the Hitachi microscope.

3. Results and Discussion

Figure 1 illustrates the characteristic morphology of the sintered cermets, where it is clearly shown that the cermets with higher Ta contents exhibited the characteristic core–rim microstructure. However, this core–rim microstructure presented an inverse contrast (the rim exhibited a darker contrast than the core) compared to that generally observed in the literature. Both core and rim were composed of $Ti_xTa_{1-x}C_{0.73}N_{0.27}$ solid solutions, but the rim had a composition that was richer in Ti. This has been confirmed via semi-quantitative EDS-SEM analyses and has been reported previously **[19]**. The presence of the core-rim microstructure diminished as the Ta content decreased, and it was not observed in cermets without Ta (sample Ti100), as expected. It was also observed that the size of the ceramic particles was reduced by increasing the Ta content. More extensive chemical and microstructural characterizations of these cermets have been described elsewhere **[18]**. It should be noted that the binder phase in these cermets was not composed of elemental Co but of Ti-Ta-Co intermetallic compounds with stoichiometries of 1:1, $(Ti_{1-x}Ta_x)Co$, and 1:2, $(Ti_{1-x}Ta_x)Co_2$ [**18**].

Figure 2a shows the thermogravimetric (TG) plots recorded during the isothermal oxidation at 900 ºC of the cermets in Table 1. A continuous weight gain (expressed in mg/cm^2) with time was observed for all samples. However, the TG profiles indicate that the presence of Ta was beneficial to improving the oxidation resistance of the cermets. When samples Ti100 and Ti99 are compared, it can be observed that by adding only a small amount of Ta (2.33 wt%, which is equivalent to substituting 1 at% of Ti with Ta in the ceramic phase), the oxidation resistance was remarkably improved; the specific weight gain caused by oxidation was reduced by 67.3 %. By increasing the Ta content, the oxidation

resistance was further enhanced, and a dramatic reduction of the weight gain (96.3 %) was observed in sample Ti80. To facilitate comparison between the cermets, the weight gain after the 48 h of oxidation is shown in Table I. As the different cermets have different weight balances associated with oxidation, the percentage of oxidation, assuming TiO_2, Ta_2O_5 and Co_3O_4 to be the fully oxidized species, is also shown in Table I.

The oxidation TG curves in Figure 2a show that the oxidation rate decreases with time following a power-law behavior. The oxidation curves were fitted using the OriginPro software package and the following general oxidation-rate equation:

$$\left(\frac{\Delta m}{S}\right) = k_n\, t^n + C \qquad (1)$$

where Δm is the weight gain, S is the surface area of the cermet, t is the oxidation time, k_n is the rate constant, n is the oxidation exponent, and C is a constant that accounts for any oxidation occurring prior to reaching the isothermal regime. The values for the exponent n calculated for the different cermets were in the range of 0.47–0.58, which is fully consistent with parabolic oxidation kinetics. This is confirmed in Figure 2b, where an excellent linearity is shown for the specific weight gain versus $t^{0.5}$ plots. The parabolic rate constants, k_p, were calculated for all cermets from these linear plots and are shown in Table II. The values of these rate constants reflected the effectiveness of the addition of Ta in improving the oxidation resistance of the cermets. For instance, the k_p value for the Ti80 cermet is three orders of magnitude lower than the one for Ti100 (Table II).

The parabolic kinetic law (as well as the linear and logarithmic laws) is a basic and simple model that was developed to explain the oxidation behavior in pure metals. However, although practical oxidation studies reported in the literature generally involve more complicated systems [**20**], in which even selective oxidation may be observed [**21**],

nearly parabolic oxidation rates have been found in many studies [**22-24**]. Even if the cermets have a multiphasic and multicomponent nature, the parabolic behavior displayed in Figure 2b for all of them is a clear indication of the formation of a compact and continuous oxide-scale layer on the surface of the cermets, and the thickness of the scale increased over time, so that the one-dimensional diffusion of reacting species through this protective layer became the rate-controlling mechanism.

Figure 3 shows SEM micrographs of the cross sections of the cermets after 48 h of oxidation at 900 ºC. These micrographs confirm the TG measurements, and a remarkable reduction in the thickness of the oxide scale was observed as the Ta content increased. A uniform and compact scale with no spallation was observed. The integrity and shape of the specimens were always maintained after oxidation. Only the size was slightly increased in those cermets that suffered greater oxidation because of the higher molar volume of the oxide scale that developed compared with the molar volume of the cermet.

The SEM micrographs in Figure 3 illustrate that not only an oxide scale was formed during oxidation; beneath the dense scale, a degraded region was observed, which is characteristic of internal oxidation phenomena. The voids and porosity observed in this degraded zone were the result of preferential oxidation (as will be shown later) and the formation of volatile species because of the oxidation of the carbonitride particles. It was observed that this porosity tended to collapse and concentrate at the interface with the dense oxide scale. In the Ti100 cermet, the extent of the internal degradation was as significant as the cermet wastage caused by scaling. In the Ti99 cermet, this degraded region was significantly reduced, and with further addition of Ta (as was observed with the oxide scale), a marked improvement was observed in terms of not only the extent of this region but also the porosity content. Any evaluation of the oxidation resistance must take into

account the presence of this degraded internal region to avoid potential shortcomings in the analysis that can result if the oxidation resistance is solely tested on the basis of the scaling behavior or the weight change. The thickness affected by oxidation, including both the compact oxide scale and the degraded subsurface region, is summarized in Table II for the different cermets.

The nature of the oxide scale that was formed after oxidation was analyzed via XRD measurements performed on the external surfaces of the cermets (Figure 4a). The unoxidized cermet constituents (ceramic and binder phases) were not detected in these XRD patterns, even in the Ti80 cermet, where, as observed from the SEM image in Figure 3, the oxide scale was only 11 μm thick. This is an indication that the penetration depth of the X-ray radiation in the oxidized cermets was below this value. Thus, the XRD patterns in Figure 4a can provide information only for the most external surface layer of the scale. The XRD patterns were assigned by comparison to the ICDD-PDF database. The assignment of the less intense XRD peaks was difficult because of the existence of preferential orientations.

Figure 4a indicates that the composition of the external layer was affected by the Ta content. Cobalt oxide phases, mainly CoO and, to a minor extent, Co_3O_4, were observed in the Ti100 cermet. The same cobalt oxides were detected in Ti99, but with a higher proportion of Co_3O_4. Minor peaks associated with Co_2TiO_4 spinel were also detected in this sample. In these two cermets, the low intensities of the peaks corresponding to the TiO_2-based rutile phase, which is supposed to be one of the main products of oxidation, suggest that this phase was located under an external layer that was rich in cobalt oxides. As the Ta content increased, the CoO and Co_3O_4 XRD peaks tended to diminish, whereas those of

Co_2TiO_4 and rutile increased. Thus, in the Ti95 cermet, CoO, Co_3O_4, Co_2TiO_4 and TiO_2 were clearly detected. However, CoO and Co_3O_4 were not observed in the Ti90 and Ti80 cermets. Only Co_2TiO_4, TiO_2 and, in a lower proportion, a new phase with an ilmenite structure ($CoTiO_3$) were detected at the surfaces of these cermets. These results suggest that the presence of Ta enhances the formation of double Ti-Co oxides instead of single cobalt oxides. In the cermets with higher Ta content, a shift toward lower angles was observed for the XRD peaks corresponding to the rutile phase, most likely because of the partial substitution of Ti^{4+} by Ta^{5+} in the rutile lattice. Therefore, the rutile phase could be defined as a solid solution with a $Ti_xTa_{1-x}O_2$ stoichiometry.

When XRD measurements were performed after crushing the oxidized samples (bulk analysis), the XRD patterns (Figure 4b) were in agreement with the SEM observations and the TG measurements. The presence of the original ceramic ($Ti_xTa_{1-x}C_{0.5}N_{0.5}$) and binder ($Ti_{1-x}Ta_xCo$ and $Ti_{1-x}Ta_xCo_2$) components was observed for all the cermets. Moreover, the rutile-based oxide, which was the main oxidized phase observed (instead of the Co-containing oxides), was a major phase only in the Ti100 and Ti99 cermets, which had lower oxidation resistances. In contrast, the presence of this oxide was almost negligible in the Ti95 and Ti90 cermets and practically nonexistent in the Ti80 cermet, the cermet with the highest oxidation resistance. The XRD patterns after oxidation for these three cermets (Ti95, Ti90 and Ti80) were practically identical to the patterns recorded before oxidation [**18**].

To obtain more information about the oxidation behavior of the cermets and the nature of the oxidized phases, EDS-SEM mappings and punctual analyses were performed in the oxidized cermets from the external surface layers toward the centers of the specimens. First, EDS mappings were obtained at the outer layers of the different cermets

(Figure 5). Before analyzing the results in Figure 5, it should be noted that the studied areas correspond to a small fraction of the total region that was affected by oxidation in the Ti100 and Ti99 cermets, while they cover practically the entire region affected by oxidation in the Ti95, Ti90 and Ti80 cermets, as confirmed by the elemental maps of O. Figure 5 shows that independent of the cermet, the dense Ti-rich oxide scale was overlaid by a thin layer that contained a high concentration of cobalt (Co-containing oxide phases), whose thickness decreased with increasing Ta content. These results are in full agreement with the XRD patterns shown in Figure 4a. The formation of this Co-rich layer on the surfaces of the cermets, which was driven by a preferential oxidation process, as shown later, induced an inner Co-depleted zone composed only of the rutile-based phase (Figure 5). This can also be observed in Figure 6, where details of the dense oxide scale and the internal oxidation region are shown for the different oxidized cermets.

The SEM images in Figures 5 and 6 exhibit different contrasts in both the dense oxide scale and the internal degraded region, indicating the existence of zones with different chemical compositions. To clarify this aspect of the cermets, semi-quantitative EDS analyses were conducted at different locations (marked with numbers in Figure 6), and representative results are shown in Table III, which also indicates the nature of the phases that best suits the results of the EDS analyses. These results confirmed the existence of mixed Co-Ti oxides (Co_2TiO_4 and/or $CoTiO_3$) at the surfaces of the oxidized Ti80, Ti90 and Ti95 cermets. It is worth noting that the mixed oxide that was richer in Ti ($CoTiO_3$) was detected at the interface region with the rutile-based oxide (bottom side of the external layer). Stoichiometries close to CoO and Co_3O_4 were only observed in the Ti100 and Ti99 cermets. In these cermets, cobalt titanate phases were also detected at the interface with the rutile phase and in the close vicinity of the Co-rich layer, appearing as islands embedded in

the rutile phase (more clearly visible in Figure 5). However, in the Ti100 cermet, underneath the dense Co-depleted rutile scale, which was 75 μm thick on average, and before reaching the degraded internal oxidation region, a new dense zone composed of a mixture of rutile and Co_2TiO_4 or $CoTiO_3$ phases was clearly detected (Figure 6). The nature of these phases was corroborated by the EDS measurements (Table III).

The coexistence of these different Co-containing oxide phases is not surprising when the binary CoO/Co_3O_4-TiO_2 phase diagram in air is considered [**25**]. Of the two stable cobalt oxides, CoO and Co_3O_4, CoO is the more stable phase above 900 ºC. Moving from the Co-containing corner to regions richer in Ti, the formation of the Co_2TiO_4 spinel phase and later the $CoTiO_3$ ilmenite phase is possible, and there exist wide compositional regions where both phases can coexist. In addition, Co_3O_4 and Co_2TiO_4 have the spinel structure and form a solid solution. It has also been reported that both Co_2TiO_4 and $CoTiO_3$ can be obtained by heating stoichiometric mixtures of Co_3O_4 and TiO_2 [**26,27**].

The SEM observations in Figure 5 and the EDS analysis in Table III suggested that the porosity of the external Co-rich layer decreased as its nature changed from single (CoO or Co_3O_4) to mixed (Co_2TiO_4 and/or $CoTiO_3$) oxides. The formation of ternary oxides during the oxidation treatment caused by reactions between the single oxides (CoO and/or Co_3O_4 with the rutile-based phase) may aid in properly densifying this external layer by providing suitable protection against oxidation. In the Ti90 and Ti80 cermets, where the oxidation was dramatically reduced, it is possible that the external cobalt oxide layer formed during oxidation was thin enough to completely react with the rutile during the 48 h oxidation process to yield the external titanate layer. In fact, the titanate layer in the Ti80 and Ti90 cermets was only 2-3 μm thick, which was similar to the thickness of the titanate

layer observed in the Ti100 and Ti99 cermets located at the interface between the cobalt oxide and rutile phases.

The EDS analysis presented in Table III demonstrated that the Ta content in the titanate phases at the external layer was practically nonexistent, even in those cermets that contained a large amount of Ta. Moreover, a Ta compositional gradient was also observed in the rutile phase from the external to the internal region of the dense scale, as exemplified by the Ti90 cermet in Table III (analyses 2, 3 and 4). The most external rutile phase was practically free of Ta. Moving inwards, the rutile was progressively enriched in this element, confirming the formation of a $Ti_xTa_{1-x}O_2$ solid solution. A Ti/Ta ratio in agreement with the nominal composition of the cermet was evident in the rutile phase near the internal oxidation region. This compositional gradient suggested the existence of outward Ti diffusion, while Ta did not seem to exhibit significant mobility through the oxide scale.

The EDS analysis confirmed for all cermets that the internal oxidation region beneath the dense oxide scale was composed of rutile ($Ti_xTa_{1-x}O_2$) and elemental Co (Table III). This is illustrated in Figure 7, where representative EDS mappings performed in this region for the Ti95 and Ti100 cermets are shown. This region corresponds to a transient oxidation stage where all $Ti_xTa_{1-x}C_{0.5}N_{0.5}$ ceramic particles have been oxidized. In addition, the presence in this region of elemental Co, not the former binder phase ($Ti_{1-x}Ta_xCo$ and/or $Ti_{1-x}Ta_xCo_2$ intermetallic compounds), indicates that Ti and Ta were preferentially oxidized in the binder. Both elements have more affinity for oxygen than Co and, therefore, reacted faster. Nevertheless, if the oxidation were prolonged, Co would also oxidize, as evidenced in the T100 cermet by the presence of cobalt titanates in the dense oxide scale near the internal oxidation region.

It is possible that this preferential Ti and Ta oxidation was the cause of the Co-rich outer layer. At the beginning of the oxidation, Ti and Ta oxidize preferentially in the binder, and the released Co is able to migrate outwards, creating the outer Co-rich layer and the Co-depleted zone. As the oxidation proceeds, this external Co is also oxidized to CoO or Co_3O_4, and it finally reacts with the rutile phase to form the spinel and ilmenite phases. Once the rutile-based scale is densified, Co cannot migrate further toward the exterior, and a new inner region containing both rutile and oxidized cobalt phases can form, as observed in the Ti100 cermet (Figure 6).

SEM observations conducted exactly in the region where the internal oxidation is incipient reflected that the oxidation tends to progress through the binder phase. This is more clearly visible in Figure 8, where EDS mappings in this region are presented for the Ti80, Ti95 and Ti99 cermets. It was observed that the Ti and Ta in the binder are oxidized first, even before the $Ti_xTa_{1-x}C_{0.5}N_{0.5}$ particles, suggesting that the advancement of the oxidation front proceeds through the binder phase, which seems to provide easier access to incoming oxygen than the ceramic particles.

The improvement in the oxidation resistance observed in the present work for cermets containing Ta is especially important when compared with the oxidation behavior of typical hard metals and cemented carbides [**28-31**]. These materials are rather unstable under oxidizing conditions at temperatures above 600-650 ºC, for which they suffer a pronounced degradation in strength [**29**]. It is usually found that the oxidation kinetics obey linear rate laws [**28,29**] as a consequence of the nature of the oxide scale that forms, which contains non-protective WO_3. The oxidation resistance of cemented carbides has been improved by partially replacing WC with other cubic refractory carbides [**30**] or increasing the metallic binder content [**31**]; in this manner, the proportion of WO_3 in the oxide scale

can be reduced, thus reducing the porosity, as well. However, the detrimental effect on the oxidation resistance that arises from the presence of WC is a serious drawback for the use of these materials in high-speed machining processes. Therefore, cermets that possess good stability in typical working oxidizing environments are potential candidates for these applications. In this sense, the oxidation resistance found for cermets that contain approximately 10 wt% of Ta, equivalent to the Ti95 cermet, can satisfy the requirements for applications up to temperatures of 900 ºC.

The cermets that contain Ta also exhibited better performance in comparison with other studies of the oxidation behavior of Ti(C,N)-based cermets [**13-16**]. In [**13,14**], a cermet with a nominal composition in wt% of 76.4$TiC_{0.5}N_{0.5}$ + 15.3(WC–5Co) + 6.2Ni + 2.1Co was studied, and it was shown that its oxidation followed a linear kinetics behavior. This was a clear indication of the formation of a non-protective oxide scale, which is highly undesirable. After 20 h of oxidation at 900 ºC in static air, the authors observed the formation of a 20 μm thick TiO_2-based scale and an intermediate reaction layer of similar dimensions. It is interesting to note that as observed in the present work, on the outer oxidized surface, a shallow layer containing mixed oxides ($NiCoO_2$ and $NiTiO_3$) was detected. The presence of WC in this cermet accounted for its low thermal stability in oxidizing environments. The low mass gain observed of 2.5 mg/cm^2 was attributed to the mass loss associated with the volatilization of WO_x species.

In [**15,16**], two more complex cermets with nominal compositions in wt% of 34.1TiC–10TiN–16Mo–6.5WC–0.8C–0.6Cr_3C_2–32Ni and 34.1TiC–10TiN–16Mo–6.5WC–0.8C–0.6Cr_3C_2–25.6Ni–6.4Cr were studied. Mass gains of 1.18 mg/cm^2 and 1.51 mg/cm^2 were found after oxidation at 900 ºC for 2 h in the cermets without and with Cr in the

binder, respectively, even though the release of volatile molybdenum and tungsten oxides was evident. In these cermets, the formation of a dense oxide scale and a transient layer, where the oxidation was incomplete, was also observed. Ternary oxides such as $NiTiO_3$, $NiMoO_4$ and $Cr_{0.17}Mo_{0.83}O_2$ were also detected after oxidation in the range 800-1100 ºC. Although the presence of Cr in the binder slowed the increase in oxidization with increasing time and temperature, the authors observed the presence of porosity in the oxide scale and spallation, which was evidence of the detrimental effect of the presence of Mo and/or WC as components of the cermets.

4. Conclusions

The inclusion of Ta as a component in Ti(C,N)-based cermets is an effective method of improving their oxidation resistance. It was observed that the oxidation rate was strongly dependent on the Ta content and was dramatically reduced, along with the thickness of the oxide scale layer, as the Ta content in the cermet increased. The evolution of the oxidation weight gain with time obeys a parabolic behavior, which implies the formation of an oxide protective layer. It was found that the parabolic constant rate decreased as the Ta content increased. Ta seems not to modify the oxidation mechanism of cermets but only to reduce its extent.

The presence of Ta in the ceramic particles and in the binder may reduce the solubility and transport of oxygen in both phases, thereby inhibiting the oxidation of cermets. Furthermore, the incorporation of Ta^{5+} in the Ti^{4+}-containing rutile scale, leading to the formation of a $Ti_xTa_{1-x}O_2$ solid solution, may also reduce the oxygen vacancies and, hence, the oxygen-ion diffusivity through the oxide scale. Moreover, Ta appears to accelerate the formation of cobalt titanates at the surfaces of cermets, which reduces the porosity of the outermost region of the oxide scale and improves the densification of the rutile-based scale. These phenomena may also explain the enhanced oxidation resistance observed in these materials.

Acknowledgments

This work was supported by the Spanish government under grant No. MAT2011-22981, which is financed in part by the European Regional Development Fund of 2007–2013. E. Chicardi and J. M. Córdoba were supported by CSIC through JAE-Pre and JAE-Doc grants, respectively, which are financed, in part, by the European Social Fund (ESF).

References

[1] Y. Zheng, W.J. Liu, S.X. Wang, W.H. Xiong, Ceram. Int. 30 (2004) 2111–2115.

[2] L. Lindau, K.G. Stjernberg, Powder Metall. 4 (1976) 210–213.

[3] H. Yoshimura, T. Sugisawa, K. Nishigaki, H. Doi, Int. J. Refrac. Met. Hard Meter. 12 (1983) 170–174.

[4] J. Zackrisson, H.O. Andren, Int. J. Refrac. Met. Hard Mater. 17 (1999) 265–273.

[5] J. Kim, M. Kim, M. Kang and S. Kang. Material properties and tool performance of Ti-based solid solution cermets for micro end-mill applications. Int. J. Refrac. Met. Hard Mater. 36 (2013) 278–282.

[6] Pastor H. Titanium-carbonitride-based hard alloys for cutting tools. Mat. Sci. Eng. A 1988;105:401-9.

[7] Ettmayer P, Kolaska H, Lengauer W, Dreyert K. Ti(C, N) cermets—metallurgy and properties. Int J Refract Met Hard Mater 1995;13:343-51.

[8] Y.R. Liu, J.J. Liu, B.L. Zhu, Z.B. Luo, H.Z. Miao, Wear 210 (1997) 39.

[9] N.A. Abukhshim, P.T. Mativenga, M.A. Sheikh, Int. J. Mach. Tools Manuf. 46 (2006)782.

[10] A. Bellosi, F. Monteverde, R. Calzavarini, C. Zancolo, Int. J. Refract. Met. Hard Mater. 19 (2001) 191-202.

[11] Tretyakov VL, Mashevskaya VL. Effect of tantalum on the properties and microstructure of hard alloys based on titanium carbonitride. Powder Metall Met Ceram 38 (1999) 64-67.

[12] D. S. Park, C Park, Y.D. Lee. Oxidation of Ti(C,N)-based ceramics exposed at 1373 K in air. J. Am. Ceram. Soc. 83 (2000) 672-674.

[13] F. Monteverde, A. Bellosi, Corros. Sci. 44 (2002) 1967.

[14] F. Monteverde, V. Medri, A. Bellosi, Mikr.ochim. Acta 138–139 (3–4) (2002) 97.

[15] Q. Yang, W. Xiong, S. Li, H. Dai and J. Li. Characterization of oxides scales to evaluate high temperature oxidation behavior of Ti(C,N)-based cermets in static air. J. All. Comp. 506 (2010) 461-467.

[16] Q. Yang, W. Xiong, S. Li, Z. Yao and X. Chen. Early high temperature oxidation behavior of Ti(C,N)-based cermets in air. Corros. Sci. 52 (2010) 3205-3211.

[17] J.M. Córdoba, E. Chicardi, F.J. Gotor. Development of multicomponent–multiphase materials based on (Ti,Ta,Nb)C_xN_{1-x} carbonitride solid solutions. Chem. Eng. J. 192 (2012) 58–66.

[18] E. Chicardi, Y. Torres, J.M. Córdoba, P. Hvizdoš and F.J. Gotor, Effect of Tantalum content on the microstructure and mechanical behaviour of cermets based on (Ti_xTa_{1-x})(C_yN_{1-y}) solid solutions. Mater. Design 53 (2014) 435–444.

[19] Chicardi E, Córdoba JM, Sayagués MJ, Gotor FJ. Inverse core-rim microstructure in (Ti,Ta)(C,N)-based cermets developed by a mechanically induced self-sustaining reaction. Int. J. Refract. Met. Hard Mater. 2012; 31: 39-46.

[20] F. Gesmundo, B. Gleeson, Oxid. Metals. 44 (1-2) (1995) 211–237.

[21] D.J. Young, B. Gleeson, Corros. Sci. 44 (2002) 345–357.

[22] E. Butchereit, K.G. Nickel, A. Muller. Precursor-Derived Si-B-C-N Ceramics: Oxidation Kinetics. J. Am. Ceram Soc. 84 [10] (2001) 2184–2188

[23] N. Babu, R. Balasubramaniam, A. Ghosh. High-temperature oxidation of Fe3Al-based iron aluminides in oxygen. Corros. Sci. 43 (2001) 2239-2254

[24] D. Yao, R. Cai, C. Zhou, J. Sha, H. Jiang. Experimental study and modeling of high temperature oxidation of Nb-base in situ composites. Corros. Sci. 51 (2009) 364–370

[25] K.T. Jacob, G. Rajitha. Role of entropy in the stability of cobalt titanates. J. Chem. Thermodynamics 42 (2010) 879–885

[26] M. Inagaki, S. Naka. Decomposition of Co_2TiO_4 spinel below 1000 K. J. Solid State Chem. 13 (1975) 365-367.

[27] P.S. Anjana, M.T. Sebastian. Synthesis, Characterization, and Microwave Dielectric Properties of $ATiO_3$ (A = Co, Mn, Ni) Ceramics. J. Am. Ceram Soc. 89 (2006) 2114-2117.

[28] Voitovich V.B., Sverdel V.V., Voitovich R.F., Golovko E.I. Oxidation of WC-Co, WC-Ni and WC-Co-Ni hard metals in the temperature range 500-800ºC. Int. J. Refract. Metals Hard Mater. 1996: 14: 289-295.

[29] B. Casas, X. Ramis, M. Anglada, J.M. Salla, L. Llanes. Oxidation-induced strength degradation of WC-Co hardmetals. Int. J. Refract. Metals Hard Mater. 19 (2001) 303-309.

[30] C. Barbatti, J. Garcia, P. Brito, A. Rita Pyzalla. Influence of WC replacement by TiC and (Ta,Nb)C on the oxidation resistance of Co-based cemented carbides. Int. J. Refract. Metals Hard Mater. 2009: 27(4): 768-776

[31] M. Aristizabal, J.M. Sanchez, N. Rodriguez, F. Ibarreta, R. Martinez. Comparison of the oxidation behaviour of WC–Co and WC–Ni–Co–Cr cemented carbides. Corros. Sci. 2011: 53: 2754-2760

Figure Captions

Figure 1. SEM micrographs of the cermets before oxidation showing their characteristic microstructure.

Figure 2. The evolution of the specific weight change (mg/cm^2) with time during the oxidation in air at 900 ºC of the studied cermets (points: experimental data; line: fitted data). a) Normal plot and oxidation exponent, *n*, of the power law and b) linear parabolic plot. Inserts show the low value data of more oxidation resistant cermets.

Figure 3. SEM micrographs showing the oxide scale and the internal oxidation degradation of the cross sections of the cermets oxidized in air at 900 ºC for 48 h.

Figure 4. XRD patterns of the cermets after oxidation in air at 900 ºC for 48 h (a) corresponding to the exposed surface and (b) after hand-grinding the specimens (bulk analysis). (○) CoO; (⊗) Co_3O_4; (∗) TiO_2; (♦) Co_2TiO_4; (■) $CoTiO_3$; (□) $Ti_xTa_{1-x}C_{0.73}N_{0.27}$; (▲) $Ti_{1-x}Ta_xCo$; (●) $Ti_{1-x}Ta_xCo_2$.

Figure 5. SEM-EDS elemental mappings performed at the outer regions of the oxide scale of the cermets oxidized in air at 900 ºC for 48 h.

Figure 6. SEM micrographs showing different zones of the oxide scale and internal oxidation regions of the cermets oxidized in air at 900 ºC for 48 h. The numbers in this

figure mark the zones analyzed via EDS, and the results of this analysis are shown in Table III.

Figure 7. EDS mappings for the Ti95 and Ti100 cermets performed in the internal oxidation region beneath the dense oxide scale; this internal region was composed of rutile ($Ti_xTa_{1-x}O_2$) and elemental Co.

Figure 8. EDS mappings for the Ti80, Ti95 and Ti99 cermets in the region where the internal oxidation is incipient, showing that the Ti and Ta of the binder are oxidized before the $Ti_xTa_{1-x}C_{0.5}N_{0.5}$ particles.

Table I. Nominal compositions of the studied cermets as well as the specific weight gain and percentage of full oxidation after annealing at 900 ºC in static air for 48 h.

Cermet	Ta content (wt%)	Nominal composition	Weight gain (mg/cm²)	Oxidation (%)
Ti100	0	80 wt% $TiC_{0.5}N_{0.5}$ + 20 wt% Co	48.13	44.2
Ti99	2.33	80 wt% $Ti_{0.99}Ta_{0.01}C_{0.5}N_{0.5}$ + 20 wt% Co	15.73	18.6
Ti95	10.71	80 wt% $Ti_{0.95}Ta_{0.05}C_{0.5}N_{0.5}$ + 20 wt% Co	4.57	4.5
Ti90	19.51	80 wt% $Ti_{0.9}Ta_{0.1}C_{0.5}N_{0.5}$ + 20 wt% Co	2.80	3.3
Ti80	33.08	80 wt% $Ti_{0.8}Ta_{0.2}C_{0.5}N_{0.5}$ + 20 wt% Co	1.80	2.4

Table II. Parabolic rate constants, k_p, for the oxidation in air at 900 ºC and the thickness affected by oxidation after 48 h.

Cermet	k_p	Thickness affected by oxidation (µm)		
	($mg^2\ cm^{-4}\ s^{-1}$)	Total	Oxide scale	Internal oxidation
Ti100	1.44×10^{-2}	585	279	306
Ti99	1.45×10^{-3}	187	118	69
Ti95	9.55×10^{-5}	49	33	16
Ti90	3.68×10^{-5}	34	18	16
Ti80	1.49×10^{-5}	21	11	10

Table III. Punctual EDS analysis performed in different zones of the oxide scale and the internal oxidation region in the oxidized cermets. The numbers in Fig. 6 mark the analyzed zones.

Cermet	Zone	Description	Ti (at%)	Ta (at%)	Co (at%)	O (at%)	Approximate phase
Ti80	1	Co-rich external layer (upper side)	12.8	0.4	29.2	57.6	Co_2TiO_4
Ti80	2	Co-rich external layer (bottom side)	20.4	0.5	21.8	57.3	$CoTiO_3$
Ti80	3	Rutile-based scale	33.4	2.9	3.3	60.4	$Ti_{1-x}Ta_xO_2$
Ti80	4	Internal oxidation zone (oxide phase)	32.7	3.9	2.4	61.0	$Ti_{1-x}Ta_xO_2$
Ti90	1	Co-rich external layer	11.8	0.5	29.7	58.0	Co_2TiO_4
Ti90	2	Rutile-based scale (upper side)	36.0	0.5	2.2	61.3	TiO_2
Ti90	3	Rutile-based scale (middle side)	33.3	2.0	2.1	62.6	$Ti_{1-x}Ta_xO_2$
Ti90	4	Rutile-based scale (bottom side)	32.1	3.7	1.2	63.0	$Ti_{1-x}Ta_xO_2$
Ti90	5	Internal oxidation zone (unoxidized binder)	5.7	1.4	86.8	6.1	Co(Ti,Ta)
Ti95	1	Co-rich external layer (upper side)	15.0	0.5	28.1	56.4	Co_2TiO_4
Ti95	2	Co-rich external layer (bottom side)	24.9	0.3	18.8	56.0	$CoTiO_3/TiO_2$
Ti95	3	Rutile-based scale	34.1	1.4	1.9	62.6	$Ti_{1-x}Ta_xO_2$
Ti95	4	Internal oxidation zone (unoxidized binder)	8.2	1.0	88.0	2.8	Co(Ti,Ta)
Ti99	1	Co-rich external layer (upper side)	1.3	0.4	53.6	44.7	CoO
Ti99	2	Co-rich external layer (bottom side)	26.5	0.4	16.8	56.4	$CoTiO_3/TiO_2$
Ti99	3	Rutile-based scale	33.8	0.5	0.9	64.8	TiO_2
Ti99	4	Internal oxidation zone (oxide phase)	32.2	0.6	1.5	65.7	TiO_2
Ti99	5	Internal oxidation zone (unoxidized binder)	5.3	0.8	91.8	2.1	Co(Ti,Ta)
Ti100	1	Co-rich external layer	1.8	-	49.0	49.2	CoO
Ti100	2	Rutile-based scale	35.4	-	0.8	63.8	TiO_2
Ti100	3	Rutile/titanate scale (light contrast)	23.2	-	21.2	55.6	$CoTiO_3$
Ti100	4	Internal oxidation zone (oxide phase)	35.1	-	2.0	62.9	TiO_2
Ti100	5	Internal oxidation zone (unoxidized binder)	7.5	-	88.8	3.7	Co(Ti)

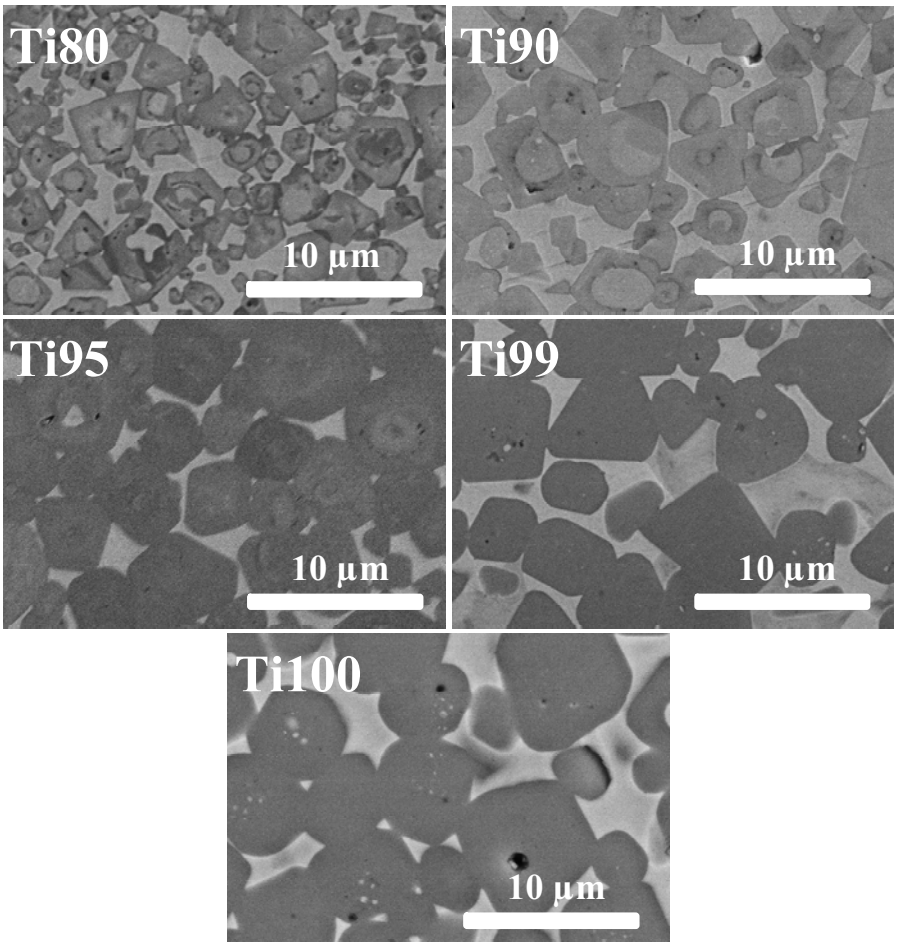

FIGURE 1

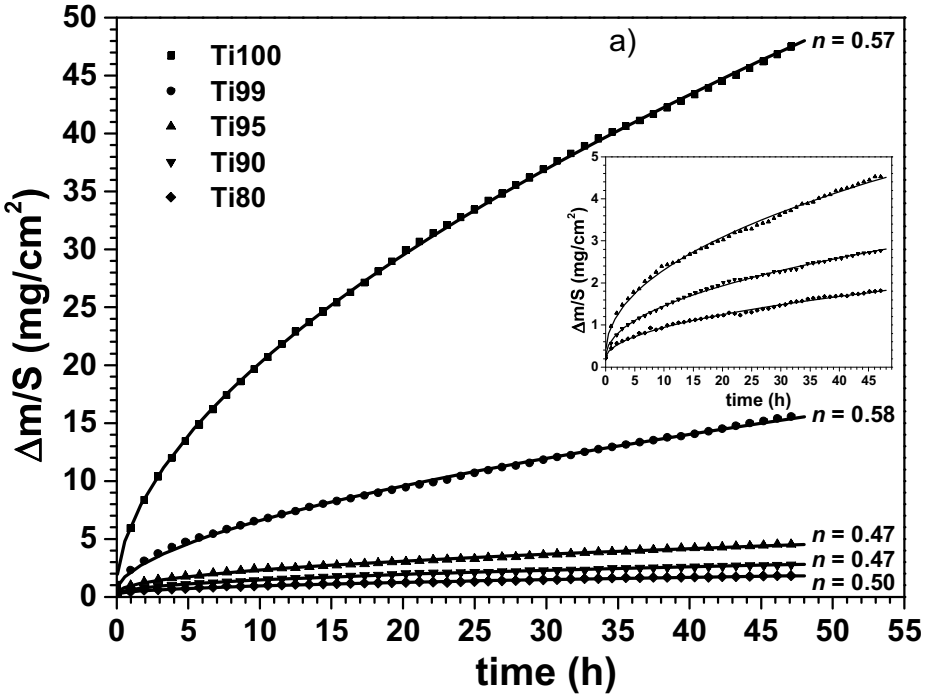
a)
Ti100
Ti99
Ti95
Ti90
Ti80
n = 0.57
n = 0.58
n = 0.47
n = 0.47
n = 0.50
Δm/S (mg/cm²)
time (h)

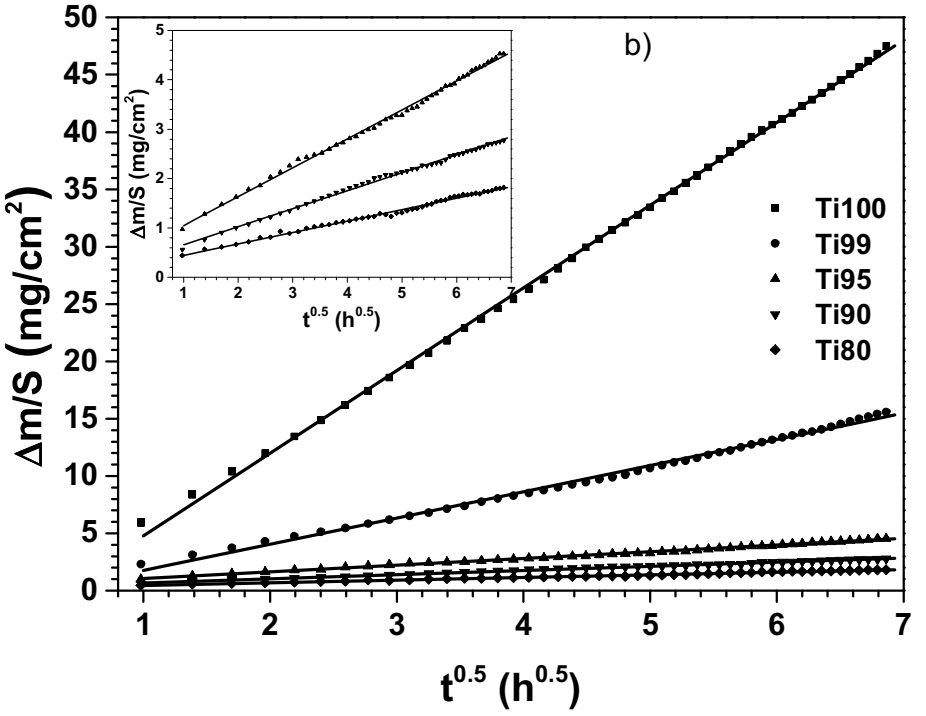
b)
Ti100
Ti99
Ti95
Ti90
Ti80
Δm/S (mg/cm²)
t^0.5 (h^0.5)

Figure 2

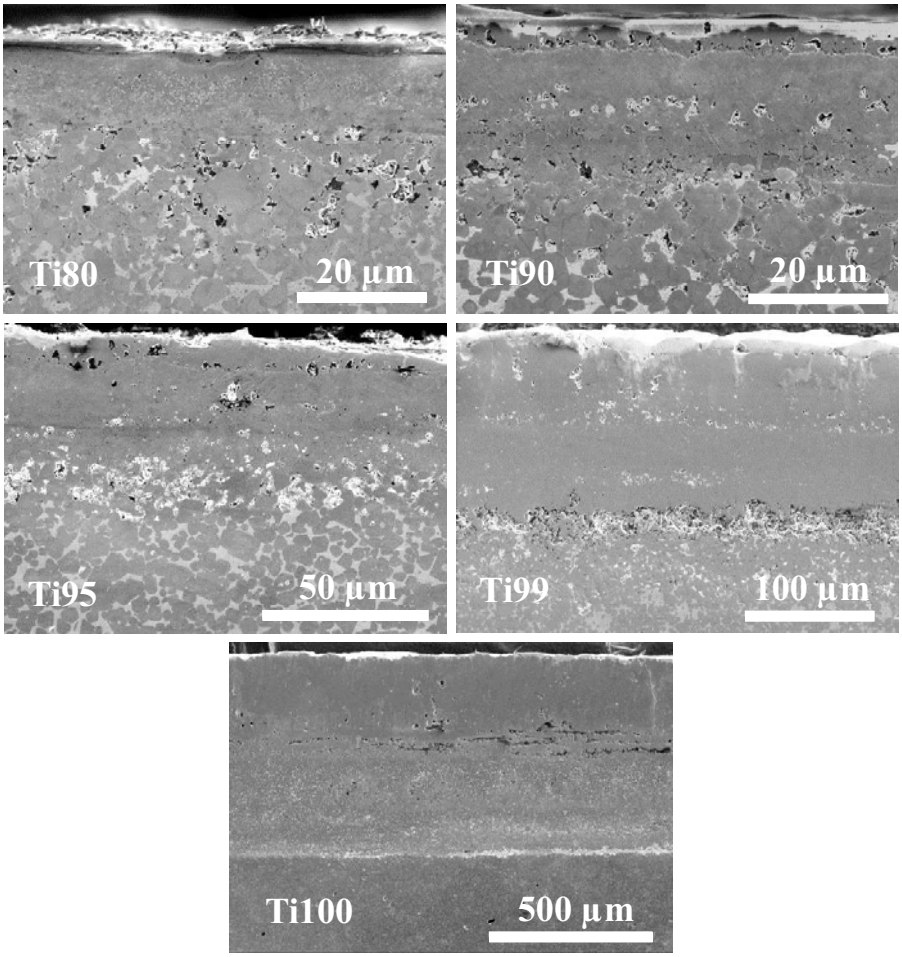

Figure 3

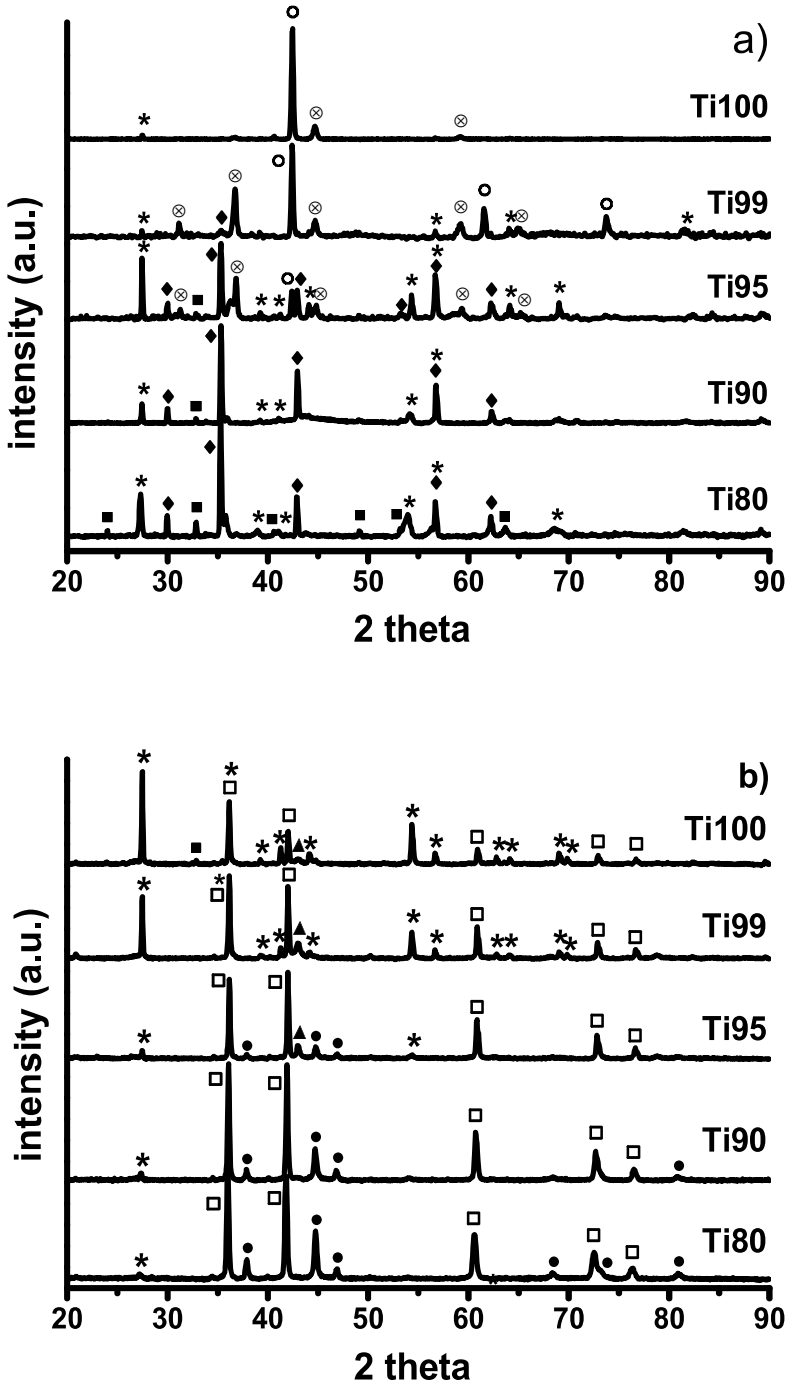
a)
Ti100
Ti99
Ti95
Ti90
Ti80
intensity (a.u.)
20
30
40
50
60
70
80
90
2 theta
b)
Ti100
Ti99
Ti95
Ti90
Ti80
intensity (a.u.)
20
30
40
50
60
70
80
90
2 theta

Figure 4

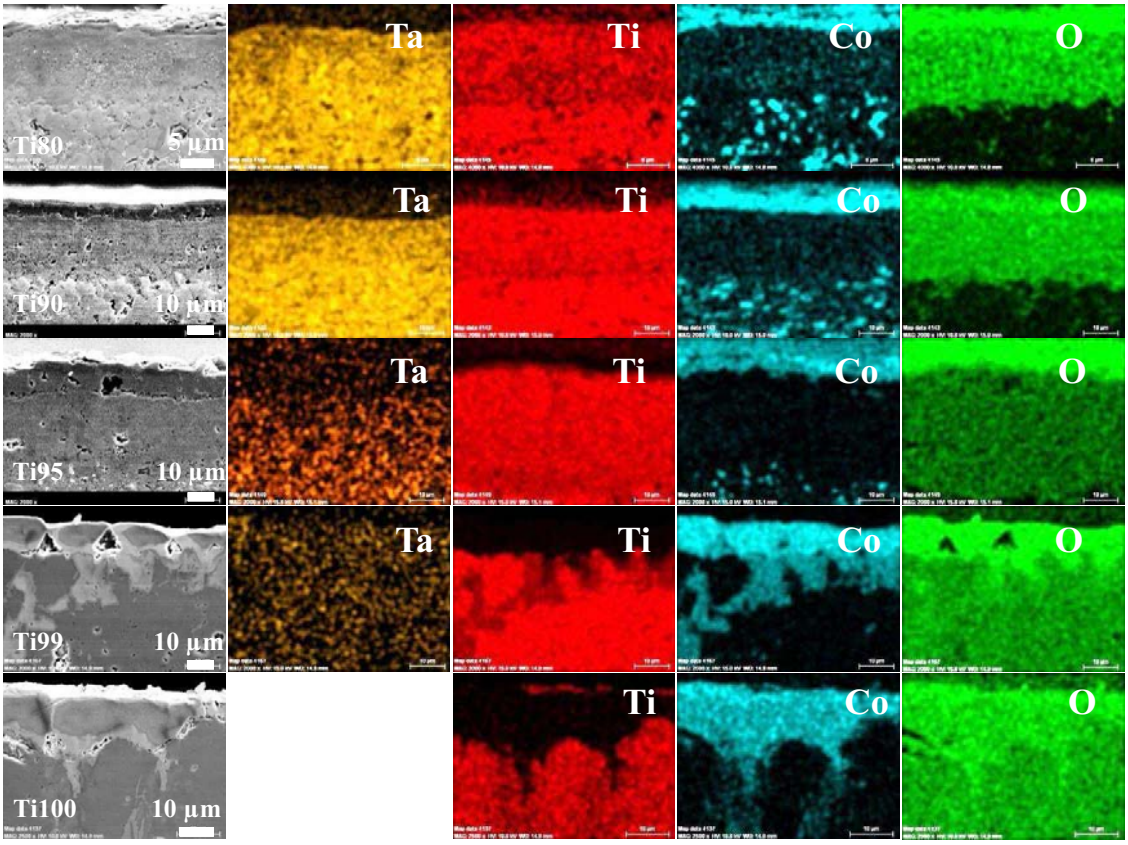
Ti80
5 µm
Ta
Ti
Co
O
Ti90
10 µm
Ta
Ti
Co
O
Ti95
10 µm
Ta
Ti
Co
O
Ti99
10 µm
Ta
Ti
Co
O
Ti100
10 µm
Ti
Co
O

Figure 5

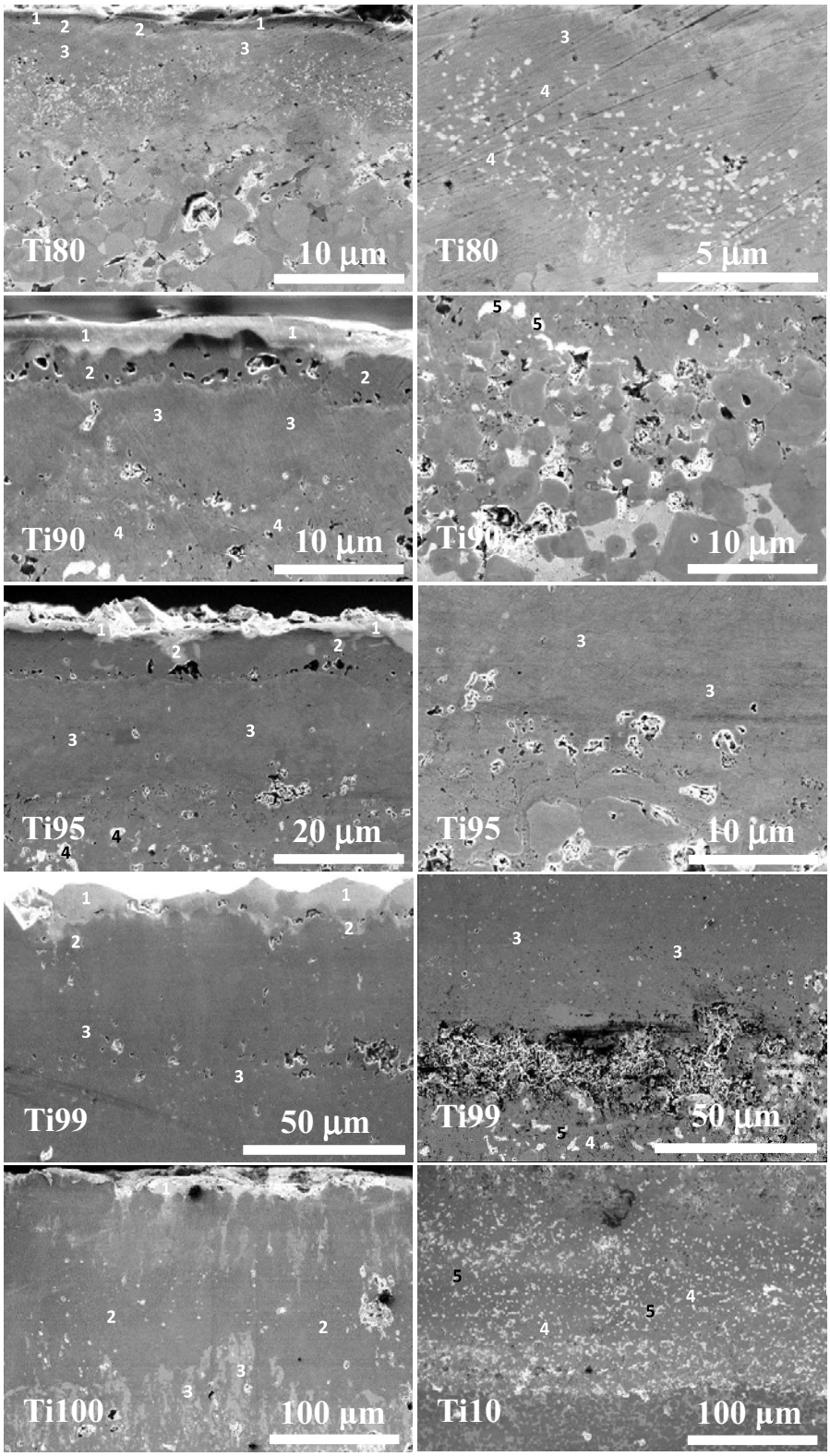
Ti80
10 µm
Ti80
5 µm
Ti90
10 µm
Ti90
10 µm
Ti95
20 µm
Ti95
10 µm
Ti99
50 µm
Ti99
50 µm
Ti100
100 µm
Ti10
100 µm

Figure 6

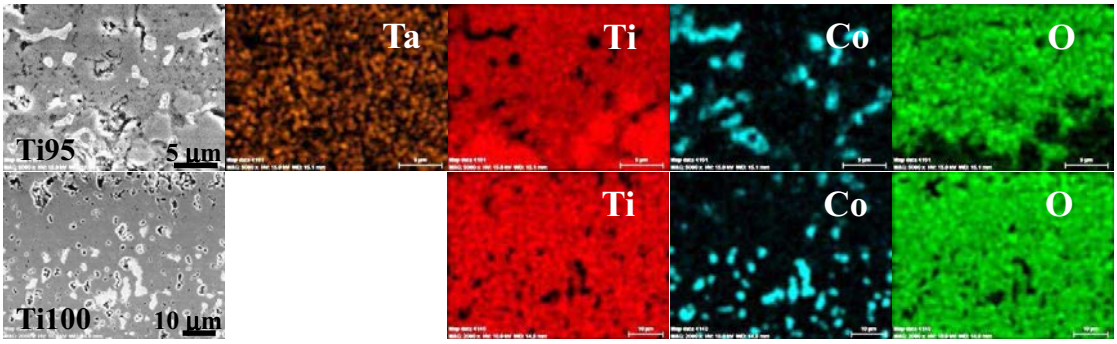

Figure 7

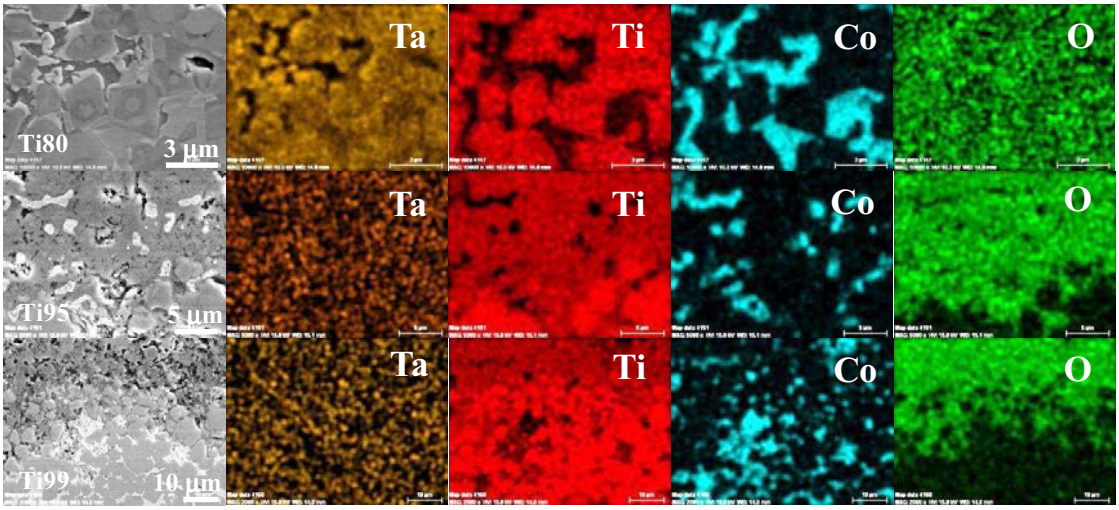

Figure 8